Integrated Orbit Determination and Maintenance in Earth-Moon Unstable Dynamics Environment

Zhou, Yang
Department of Aeronautics and Astronautics, Kyushu University

Bando, Mai
Department of Aeronautics and Astronautics, Kyushu University

Hokamoto, Shinji
Department of Aeronautics and Astronautics, Kyushu University

Wu, Panlong
School of Automation, Nanjing University of Science and Technology

出版情報：Acta Astronautica. 163 (B), pp.69-76, 2019-10. Elsevier
バージョン：
権利関係：

Integrated Orbit Determination and Maintenance in Earth-Moon Unstable Dynamics Environment

Yang Zhou[a,b], Mai Bando[a], Shinji Hokamoto[a], Panlong Wu[b]

[a] *Department of Aeronautics and Astronautics, Kyushu University, Fukuoka City 819-0395 JAPAN*
[b] *School of Automation, Nanjing University of Science and Technology, Nanjing 210094 CHINA*

Abstract

The orbit determination and maintenance are always required for space missions due to the existence of uncertainties. In an unstable orbit dynamics environment, such as libration point orbits in the restricted three-body problem, the performance of orbit determination and maintenance will be severely influenced by the unstable characteristics. This paper proposes an integrated approach for orbit determination and maintenance for spacecraft subject to an unstable dynamics environment. X-ray pulsar navigation is introduced to determine the orbit of spacecraft under the unstable dynamics environment. Then a new orbital maintenance strategy is proposed for libration point orbits mission, exploiting the effect of the hyperbolic instability of libration point orbits. Simulation results for the Earth-Moon L_2 halo orbit present the effectiveness of the integrated approach.

Keywords: Orbit determination, Orbit maintenance, Libration point orbits, X-ray pulsar navigation, Orbit uncertainty

1. Introduction

Spacecraft navigation concerns how to decrease the orbit uncertainty and obtain accurate orbit prediction in order to increase the success rate of space mission [1, 2]. This paper investigates the spacecraft navigation in an unstable dynamics environment in terms of the distribution of orbit uncertainty. In a

stable dynamics environment, for example the classic two-body problem, the growth of orbit uncertainty is along the downtrack direction of the orbit, that is along the direction of the local velocity [3]. Nevertheless, the conclusion is entirely different in the unstable dynamics environment. Scheeres studied the dynamics of orbit uncertainties in the Sun-Earth system and the simulation results presented that the orbit uncertainties are stretched out along the direction of unstable manifold of local orbit in the phase space [4, 5]. Scheeres further theoretically demonstrated that unstable manifold controls the distribution of orbit uncertainty in a 1-DOF unstable system [6].

Although conventional spacecraft navigation has been successfully applied to the past the Sun-Earth libration-point missions [7, 8], the spacecraft navigation in the Earth-Moon system seems more difficult since the instability in Sun-Earth system is weak enough for the Sun-Earth system [9]. In [10], influences of the unstable dynamics to the performance of orbit determination is studied. In [4], the ground tracking method is used to determine the spacecraft's orbit and it is indicated that the distribution of orbit uncertainty will be greatly changed after the ground tracking measurements are incorporated into. Based on the local dynamics, some basic ideas are proposed in [5] and [6] by optimizing the measurement time to increase the measurement efficiency.

In contrast to past studies, this paper introduces the X-ray pulsar navigation (XNAV) for orbit determination [11] in an unstable orbital environment, instead of using the conventional ground tracking method. XNAV is a newly developed spacecraft autonomous navigation technique, owning lots of advantages for deep space exploration [12, 13]. By incorporating XNAV measurements into Kalman filter architecture, the online autonomous navigation can be realized [14]. However, most of the literatures on XNAV concerned how to increase the performance in the stable trajectory and only a few applied XNAV to unstable orbital environment [15, 16].

Libration point orbits are proved to be suitable for space science experiment, however, instability of the libration point orbits will cause the spacecraft to drift far away from the nominal one [17]. Hence, the stationkeeping maneuver

is required to maintain the spacecraft near the nominal trajectory. Farquhar [18] first introduced the stationkeeping problem for libration-point mission and proposed several strategies for near-periodic orbits about the collinear points. The famous International Sun-Earth Explorer-3 (ISEE-3) successfully applied the stationkeeping method for about 3.5 years [19]. After that, various different types of stationkeeping methods were proposed, including the target point method [20, 21] and Floquet mode method [22, 17]. In the target point method, target points are selected along the nominal trajectory on different discrete time epochs and the maintenance maneuver is performed to force the spacecraft to be close to these target points. A weighted cost function is introduced for minimizing the total maneuver cost. On the other hand, the Floquet mode method is proposed based on the dynamical systems theory and Floquet modes. The unstable component is approximated by the eigenvector associated with unstable eigenvalue of the monodromy matrix. Then maintenance maneuver can be computed to make the projection of the error onto the unstable direction be zero, meaning that the error will not diverge along this direction. Some other stationkeeping strategies are also proposed [23]. However, these strategies have similar principle that is to eliminate the error along unstable component of the monodromy matrix and use the actual state to compute the maneuver.

In this paper, the Earth-Moon circular restricted three-body problem is considered, which preserves the essential nature of the unstable dynamics in astrodynamic problem [24] and the uncertainties are incorporated to the dynamics model. Then XNAV is applied for the orbit determination and stationkeeping maneuver is designed to maintain the spacecraft in the vicinity of the reference orbit. Spacecraft's position and velocity are estimated by the Kalman filter [25]. The estimated error and the corresponding covariance matrix are used to describe the distribution of orbit uncertainty. Considering the X-ray source is widely distributed in the whole universe, it is possible to carry out orbit determination with measurements of multiple different X-ray pulsars. It is shown that different pulsars show different orbit-determination performance, which is closely related to the local unstable dynamics.

The covariance-based orbit maintenance approach is proposed to overcome the instability of monodromy matrix approach when the estimated state is deviated from the actual state. Moreover, compared with the monodromy matrix approach and the Floquet mode approach, the covariance matrix is output by the orbit-determination filter with the state estimations, meaning the computational time of monodromy matrix can be saved.

The remainder of this paper is organized as follows. Section 2 presents the spacecraft dynamics model in the rotating and inertial frames, respectively. Section 3 gives the Orbit determination with X-ray pulsar navigation. Section 4 presents the covariance-based orbit maintenance algorithm. Section 5 presents the numerical simulation and analysis for the integrated orbit determination and maintenance approach. Followed by conclusions is in Section 6.

2. Dynamics Model

As an unstable dynamics environment, the motion of spacecraft in the Earth-Moon restricted-circular three-body problem is considered. The dynamics model is defined in the Earth-Moon barycenter synodic frame, which is normalized under the following assumptions: 1) the total mass of the Earth and Moon is 1; 2) the gravitational constant is 1; 3) the distance between the Earth and Moon is 1. Thus, the normalized dynamics model is expressed as [26]

$$\begin{cases} \ddot{x} - 2\omega\dot{y} = \dfrac{\partial U}{\partial x} \\ \ddot{y} - 2\omega\dot{x} = \dfrac{\partial U}{\partial y} \\ \ddot{z} = \dfrac{\partial U}{\partial z} \end{cases} \tag{1}$$

where

$$U = \frac{\omega^2}{2}\left(x^2 + y^2\right) + \frac{1-\mu}{r_1} + \frac{\mu}{r_2},$$

(x, y, z) is the position of the spacecraft, r_1 and r_2 are the distance of the spacecraft with respect to the Earth and Moon, μ is the gravitational constant of the Earth-Moon system and ω is the rotating speed of the Earth-Moon system.

Equation (1) is usually used for theoretical analysis and trajectory design, however, is inappropriate for orbit determination with XNAV because XNAV theory is defined in the inertial frame. Consequently, the other dynamics model in the Earth-center inertial frame is also described as following

$$\begin{cases} \ddot{x} = -\frac{\mu_E}{r^3}x + \mu_M\left(\frac{x-x_m}{r_{sm}^3} - \frac{x_m}{r_m^3}\right) \\ \ddot{y} = -\frac{\mu_E}{r^3}y + \mu_M\left(\frac{y-y_m}{r_{sm}^3} - \frac{y_m}{r_m^3}\right) \\ \ddot{z} = -\frac{\mu_E}{r^3}z + \mu_M\left(\frac{z-z_m}{r_{sm}^3} - \frac{z_m}{r_m^3}\right) \end{cases} \tag{2}$$

where (x, y, z) and (x_m, y_m, z_m) are positions of the spacecraft and Moon in the inertial coordinate respectively, and μ_E and μ_M are the gravitational constant of the Earth and Moon respectively. The other variables are defined as

$$\begin{aligned} r &= \sqrt{x^2 + y^2 + z^2}, \\ r_m &= \sqrt{x_m^2 + y_m^2 + z_m^2}, \\ r_{sm} &= \sqrt{(x - x_m)^2 + (y - y_m)^2 + (z - z_m)^2}. \end{aligned}$$

Equation (2) can be rewritten in the form of first order of differential equation as

$$\dot{X}(t) = \tilde{f}[X(t), t] = \begin{bmatrix} \dot{x} \\ \dot{y} \\ \dot{z} \\ -\frac{\mu_E}{r^3}x + \mu_M\left(\frac{x-x_m}{r_{sm}^3} - \frac{x_m}{r_m^3}\right) \\ -\frac{\mu_E}{r^3}y + \mu_M\left(\frac{y-y_m}{r_{sm}^3} - \frac{y_m}{r_m^3}\right) \\ -\frac{\mu_E}{r^3}z + \mu_M\left(\frac{z-z_m}{r_{sm}^3} - \frac{z_m}{r_m^3}\right) \end{bmatrix} \tag{3}$$

where $X = [x, y, z, \dot{x}, \dot{y}, \dot{z}]^T$. The solution of Eq. (3) can be approximated with 2nd-order accuracy as

$$\begin{aligned} X(t) =& X(t_0) + (t - t_0)\,\tilde{f}[X(t_0), t_0] + \frac{(t - t_0)^2}{2} F[X(t_0), t_0]\,\tilde{f}[X(t_0), t_0] \\ &+ O(t - t_0)^2 \end{aligned} \tag{4}$$

where

$$F[X(t_0), t_0] = \left.\frac{\partial \tilde{f}[X(t), t]}{\partial X(t)}\right|_{t=t_0} \tag{5}$$

Thus, the discrete form of Eq. (3) is geivne by the nonlinear differential equation

$$X_k = f\left[X_{k-1}, k-1\right] + W_{k-1} \tag{6}$$

where

$$f\left[X_{k-1}, k-1\right] = X_{k-1} + T \cdot \tilde{f}\left[X_{k-1}\right] + \frac{T^2}{2} \cdot \tilde{f}\left[X_{k-1}\right] \cdot F\left(X_{k-1}\right) + W_{k-1},$$

and W_{k-1} is the process noise sequence and $T = t_k - t_{k-1}$.

3. Orbit Determination with X-ray Pulsar Navigation

3.1. Extended Kalman filter

The classical extended Kalman filter (EKF) algorithm [27] is adopted to determine the spacecraft's orbit and the corresponding covariance, for the advantages of simple algorithm structure and small amount of computation.

The EKF consists of time update and measurement update as

$$\hat{X}_{k,k-1} = f\left(\hat{X}_{k-1,k-1}\right) \tag{7}$$

$$P_{k,k-1} = \Phi_{k,k-1} P_{k-1,k-1} \Phi_{k,k-1}^T + Q_{k-1} \tag{8}$$

$$K_k = P_{k,k-1} H_k^T \left[H_k P_{k,k-1} H_k^T + R_k\right]^{-1} \tag{9}$$

$$\hat{X}_{k,k} = \hat{X}_{k,k-1} + K_k\left[Z_k - h\left(X_{k,k-1}\right)\right] \tag{10}$$

$$P_{k,k} = \left[I - K_k H_k\right] P_{k,k-1} \tag{11}$$

where $\hat{X}_{k,k}$ is the state estimations and $P_{k|k}$ is the corresponding covariance, $f(\cdot)$ and $h(\cdot)$ are the dynamics model and measurement model, respectively, H_k is the measurement matrix, Q_{k-1} is the process noise matrix and R_k is the measurement noise matrix, Z_k is the actual measurements, and $\Phi_{k,k-1}$ is

the state transition matrix, which is computed by integrating the following differential equations

$$\dot{\Phi}\left(t,t_0\right)=A\left(t\right)\Phi\left(t,t_0\right),\Phi\left(t_0,t_0\right)=I \tag{12}$$

$$A\left(t\right)=\frac{\partial f\left(X,t\right)}{\partial X\left(t\right)} \tag{13}$$

In general, the state and covariance are propagated forward to the epoch of the next measurements by Eqs. (7) and (8), and then they are updated with measurement input by Eqs. (10) and (11). Unfortunately, the interval between two neighbor XNAV measurements is very long, and one-step propagation in a long interval will degrade the state and covariance predictions. Therefore, the time update of the state and covariance will be performed in a shorter interval until the next measurement updating epoch.

3.2. X-ray pulsar navigation

3.2.1. Measurement Model

The time of arrival (TOA) of the photons emitted by the X-ray pulsar is used for the orbit determination. The X-ray photons are detected by the sensor mounted on the spacecraft, and after the photons are accumulated for a period, TOA at the spacecraft can be directly estimated on the basis of epoch folding technique. The difference of TOA at two spacecrafts is used as the measurements in XNAV. In general, one spacecraft is set at the solar system barycenter (SSB) and TOA at SSB is computed by the pulse timing model. Therefore, TOA at the other spacecraft is modeled as [28]

$$\begin{aligned}t_{SC}=&t_{SSB}+\frac{n\cdot r}{c}+\frac{2\mu_s}{c^3}\ln\left|\frac{n\cdot r+r}{n\cdot b+b}+1\right|\\&+\frac{1}{2cD_0}\left[\left(n\cdot r\right)^2-r^2+2\left(n\cdot b\right)\left(n\cdot r\right)-2\left(b\cdot r\right)\right]+\delta t\end{aligned} \tag{14}$$

where t_{SC} and t_{SSB} are the TOA at the spacecraft and SSB, respectively, n is the direction of the pulsar, r is the position of the spacecraft with respect to SSB, c is the speed of the light, μ_s is the gravitational constant of the Sun, b is

the position of SSB with respect to the Sun, D_0 is the distance from the pulsar to the Earth, and δt is the measurement error, resulting from the modelling error, clock error, etc.

Generally, difference of TOAs at the spacecraft and SSB is used for measurement model construction as

$$h\left[X\left(t\right),t\right]=\left[c\left(t_{SC}^{1}-t_{SSB}^{1}\right),c\left(t_{SC}^{2}-t_{SSB}^{2}\right),...,c\left(t_{SC}^{m}-t_{SSB}^{m}\right)\right]^{T} \tag{15}$$

where t_{SC}^{i} and t_{SSB}^{i} are the TOA of i-th pulsar at the spacecraft and SSB, respectively, and m is the number of simultaneously observed pulsars. Accordingly, the meausurement model of XNAV is expressed as

$$Z_k=h\left[X_k,k\right]+V_k \tag{16}$$

where V_k is the measurement noise sequence. For EKF, the corresponding measurement matrix is defined as

$$H_k=\left.\frac{\partial h\left[X,t\right]}{\partial X}\right|_{t=t_k} \tag{17}$$

3.2.2. Accuracy Model

The performance of XNAV mostly depends on the TOA accuracy that is theoretically determined by the SNR of the pulse profile. Generally, SNR of the pulse signal is expressed as [29]

$$SNR=\frac{N_p}{\sigma_N}=\frac{F_X p_f\sqrt{A\tau}}{\sqrt{\left[B_X+F_X\left(1-p_f\right)\right]W/P+F_X p_f}} \tag{18}$$

where N_p is the pulse signal component of photon-counting, σ_N is the measurement standard deviation of pulse signal, F_X and B_X are radial fluxes of the X-ray photons and X-ray background radiation flux, respectively, A is the area of the X-ray sensor, p_f is the pulse flux ratio, W is the pulse width, P is the pulse period, and τ is the accumulating time of X-ray photons. Then the accuracy of TOA is expressed as

$$\sigma_{TOA}=\frac{0.5W}{SNR} \tag{19}$$

Therefore, the ranging measurement accuracy along the line of sight to the X-ray pulsar can be expressed as

$$\sigma_{range} = c\sigma_{TOA} \tag{20}$$

4. Orbit Maintenance Algorithm

4.1. Review of Monodromy-Based Approach

Given the error between the nominal trajectory and the actual one defined as

$$\delta X_k = \begin{bmatrix} \delta r \\ \delta v \end{bmatrix} = X_k^N - X_k \tag{21}$$

where X_k^N and X_k are the state on the nominal trajectory and actual one for the k-th epoch, respectively. Then X_k can be expressed as

$$\delta X_k = \sum_{i=1}^{6} c_i e_i \tag{22}$$

where e_i are the eigenvector of the monodromy matrix, which is determined by the state transition matrix for one period of halo orbit. The six eigenvectors are sorted in three different pairs by the corresponding eigenvalue as [30]

$$\begin{aligned} \lambda_1 > 1, \lambda_2 < 1, \lambda_1\lambda_2 = 1 \\ \lambda_3 = \lambda_4 = 1 \\ \lambda_5 = \lambda_6^*, |\lambda_5| = |\lambda_6| \end{aligned} \tag{23}$$

According to the dynamical system theory, δX_k will be stretched along the unstable component and the actual trajectory will depart from the nominal one. In fact,

$$\begin{aligned} M^n \delta X_k &= M^n \sum_{i=1}^{6} c_i e_i \\ &= \sum_{i=1}^{6} c_i M^n e_i \\ &= \sum_{i=1}^{6} c_i \lambda_i^n e_i \to c_1 \lambda_1^n e_1 \, (n \to \infty) \end{aligned} \tag{24}$$

where M is the monodromy matrix.

To eliminate the unstable component of δX_k, an impulsive velocity correction Δv should be added to satisfy

$$\delta X_k + \begin{bmatrix} 0 \\ \Delta v \end{bmatrix} = \sum_{i=2}^{6} d_i e_i \tag{25}$$

To simplify the expression for Δv, the matrix of eigenvectors is divided into four block matrices as

$$[e_1, e_2, e_3, e_4, e_5, e_6] = \begin{bmatrix} S_{11} & S_{12} \\ S_{21} & S_{22} \end{bmatrix} \tag{26}$$

where S_{ij} is 3×3 matrix. Then solution of Δv is given as

$$\Delta v = \left(S_{21} - S_{22}\left(S_{12}^{-1} S_{11}\right)\right) \begin{bmatrix} 0 \\ d_2 \\ d_3 \end{bmatrix} + S_{22}\left(S_{12}^{-1}\delta r\right) - \delta v \tag{27}$$

In Eq. (27), Δv is determined by two free variables d_2 and d_3. Therefore, $|\Delta v|$ can be minimized by seeking the extremum of the quadratic polynomial of Δv^2. The specific procedure can be found in [31].

4.2. Covariance-based approach

According to [5, 6], the extremal extensions of a linear deviation δX_k is considered. To maximize the 2-norm of δX_k, the Lagrangian is introduced as

$$L = \delta X_k^T \delta X_k - \lambda\left(\delta X_k^T P_{k,k-1}^{-1} \delta X_k - p\right) \tag{28}$$

where λ is the Lagrange multiplier, $P_{k,k-1}$ is the covariance matrix without measurement update and δX_k is assumed to lie on the surface of probability ellipsoid

$$\delta X_k P_{k,k-1}^{-1} \delta X_k^T = p \tag{29}$$

where p is an arbitrary positive real number.

Solving for the extremum of L leads the following extremal condition

$$\left[P_{k,k-1} - \lambda I\right] \delta X_k = 0 \tag{30}$$

It means it is most probably that the growth of δX_k is along the direction of eigenvector associated with the maximum eigenvalue of covariance matrix $P_{k,k-1}$.

If the motion about a periodic orbit (or equilibrium point) is considered, then the limiting uncertainty directions are aligned with the unstable manifold as shown in [4]. Therefore, it is reasonable to say that the divergent direction can be determined by the maximum eigenvector of $P_{k,k-1}$, being equivalent to the unstable eigenvector of monodromy matrix.

Based on this observation, the covariance-based orbit maintenance strategy is proposed. Similarly, the error can be expressed with another set of base as

$$\delta X_k = \sum_{i=1}^{6} \bar{c}_i \bar{e}_i \tag{31}$$

where $\bar{e}_i$ is the eigenvector of covariance matrix defined by

$$P_k \bar{e}_i = \bar{\lambda}_i \bar{e}_i \tag{32}$$

It should be noted that the properties of eigenvalues in Eq. (23) do not hold for $\bar{\lambda}_i$, and all $\bar{\lambda}_i$ are positive real value since P_k is a real symmetric matrix. Therefore, the direction of maximum δX_k is determined by the eigenvector corresponding the maximum eigenvalue. Here, $\bar{\lambda}_1$ denotes the maximum eigenvalue and the corresponding eigenvector is $\bar{e}_1$.

With the maneuver correction, the coefficient of $\bar{e}_1$ should be zero, expressed as

$$\delta X_k + \begin{bmatrix} 0 \\ \Delta \bar{v} \end{bmatrix} = \sum_{i=2}^{6} \bar{d}_i \bar{e}_i \tag{33}$$

The subsequent procedure is the same as that of monodromy-based approach.

5. Simulation and analysis

5.1. Nominal Trajectory

Computation of the nominal orbit about the Earth-Moon L_2 starts from the third-order analytical solution in [32]. However, the analytical solution cannot

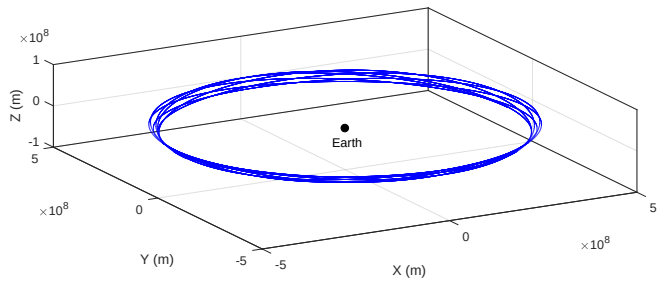

Figure 1: Trajectory in Earth center synodic frame for 12 revolutions (about 180 days).

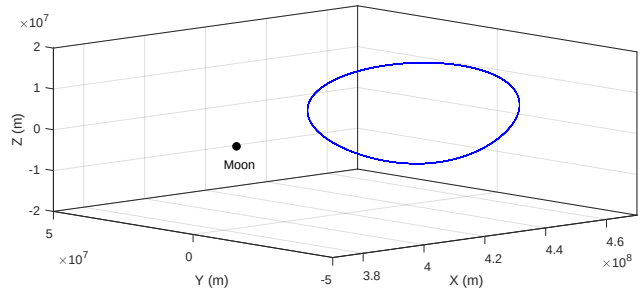

Figure 2: Trajectory in Earth center inertial frame for 12 revolutions (about 180 days).

provide the accurate initial guess for orbit propagation. Therefore, differential correction method is applied to correct the analytical solution [33]. The differential correction method utilizes the property that halo orbits are symmetrical with respect to the x-z plane. That is to say, the initial and finishing vector in every half period should be perpendicular to the x-z plane. Based on this property, the corrected initial state can be computed through multiple iterations. By propagating from the corrected initial guess, a nominal halo orbit in CRTBP is obtained, and then transformed into the Earth centered inertial frame by rotation and scaling to obtain the nominal trajectory in Earth center inertial frame. Replication of one revolution in CRTBP for multiple times provides the long-term nominal trajectory. Figures 1 and 2 show the nominal

trajectory about the Earth-Moon L_2 in the Earth centered synodic and inertial frame, respectively.

5.2. Results for orbit determination

5.2.1. Orbit determination without measurements

To investigate the distribution of the orbit uncertainty, the relationship between directions of the estimated error, the maximum orbit uncertainty and the unstable manifold is investigated. The estimated error is computed by comparing the nominal orbit with the estimated one. The maximum orbit uncertainty is defined by the maximum eigenvector of the covariance matrix. The direction of unstable manifold of a periodic orbit is locally approximated by the eigenvector associated with the unstable eigenvalue of the monodromy matrix. It is worth mentioning that the state transition matrix is defined in the rotating frame. Hence the frame transformation is applied to maintain the consistent frame with the maximum orbit uncertainty.

Figures 3 and 4 show the projection of direction of estimated error and the maximum orbit uncertainty onto the direction of the unstable manifold and downtrack, respectively. It is clear that the projection onto the direction of the unstable manifold will approach one after a certain period, meaning that the direction of estimated error and maximum orbit uncertainty are aligned with the direction of the unstable manifold.

Figure 4, on the other hand , shows that in the unstable dynamics environment, the estimated error and orbit uncertainty are not directly related to the geometry of local orbit. Instead, the unstable manifold controls the evaluation of the estimated error and orbit uncertainty in the long term. The large deviation of the estimated trajectory from the nominal trajectory shown in Fig. 5 explains the phenomenon that the projection in the end phase (after 25 days) of Fig. 3 does not hold one. It is indicated that this conclusion only holds when the estimated trajectory remains near the nominal one.

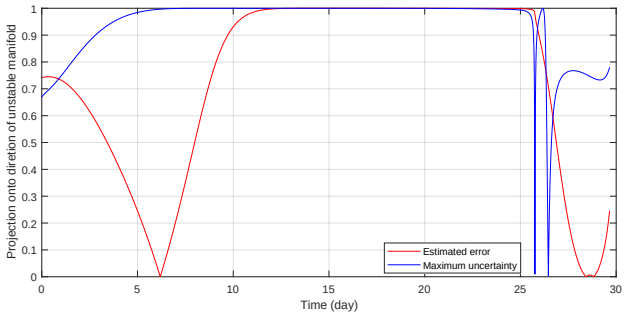

Figure 3: Projection onto direction of unstable manifold.

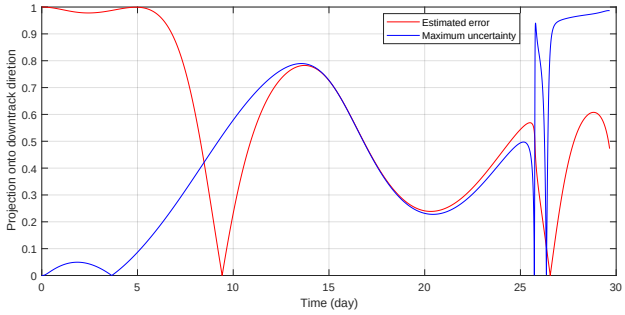

Figure 4: Projection onto downtrack direction.

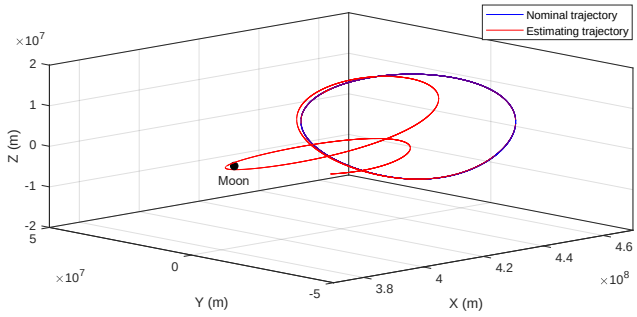

Figure 5: Estimated trajectory and nominal trajectory.

5.2.2. Orbit determination with XNAV measurements

This section investigates the effect of the XNAV measurements on the orbit uncertainty under unstable dynamics environment. Orbit determination is performed with measurements of each single pulsar. Parameters of pulsars used in the simulation are given in Table 1, and the corresponding measurement noise is computed by Eqs. (18) - (20). Other parameters in the simulation are set as: the area of X-ray detector is 1 m^2; the background radiation flux is 0.005 ph/$cm^2 \cdot s^{-1}$; The speed of light is 2.99792457×10^8 $m \cdot s^{-1}$; the gravity constant is 6.67310-11 $N \cdot m^2 \cdot kg^{-2}$; the mass of the Earth and Moon are 5.974×10^{24} kg and 7.348×10^{22} kg, respectively; the distance from the Earth to the Moon is 3.844×10^8 m.

Figures 6 to 9 show the projection of the directions of the estimated error and the maximum orbit uncertainty onto the direction of the unstable manifold with measurement updating time of 4 hours and 48 hours for B1937+21 and B1509-58, respectively. From Figs. 6 to 9, some common features can be observed. The projection tends to increase in the absence of XNAV measurements, especially in the case of longer measurement updating time, being consistent with the conclusion shown in the previous section. However, after the measurement update, the value decreases sharply. It indicates that both the estimated error and the orbit uncertainty along the unstable direction decrease, that is to say, the orbit along this direction is well determined. Figure 10 gives the angle between the direction of the unstable manifold and the pulsar line-of-sight. By comparing with Figs. 6 to 9, it can be easily found that when the angle is close to 90 deg, the effect of measurements is not clear. However, when the pulsar line-of-sight approaches the direction of the unstable manifold, the projection decreases more sharply. Particularly in Fig. 9, the orbit uncertainty does not decrease significantly after measurements because the line-of-sight of B1509-58 is almost orthogonal to the direction of unstable manifold. It can provide the indicator of judging the measurement efficiency and the criteria to select the better observations to increase the navigation performance (see [34]).

Table 1: Parameters of X-ray pulsars

Pulsar	RA (deg)	DEC (deg)	D_0 (kpc)	P (sec)	F_X (ph/cm^2·s^{-1})	P_f (%)	W (sec)
B1937+21	-65.09	21.58	3.6	0.00156	4.99×10^{-5}	86	2.1×10^{-5}
B1957+20	-60.10	20.81	1.53	0.0016	8.31×10^{-5}	60	8×10^{-5}
B1821-24	-83.87	-24.87	5.5	0.00305	1.93×10^{-4}	98	5.5×10^{-5}
B0531+21	83.64	22.01	2	0.0334	1.54	70	1.67×10^{-3}
B0540-69	85.03	-69.33	47.3	0.05037	5.15×10^{-3}	67	2.5×10^{-3}
B1509-58	48.48	-59.13	4.3	0.15023	1.62×10^{-2}	64.6	2.7×10^{-3}
J1808-3658	-87.88	-36.96	4	0.00249	0.329	4.1	5×10^{-4}
J1814-338	-86.58	-33.77	8	0.00318	9.97×10^{-2}	12	6.4×10^{-4}

Under the circumstance of different measurement updating time, for example in Fig. 6 and 7, the blue line decreases more sharply after the measurement update than the red line. This is due to the difference of measurement accuracy, that more accurate measurements can decrease the orbit uncertainty more effectively. Another interesting phenomenon is observed, for example as in the red line shown in Fig. 7. When the simulation time is on Day 3 and Day 17, the projection increases after the measurement update, which is contrary to other results. It is found from Fig. 10 that the angle of Day 3 and Day 17 is 90 deg, meaning the unstable manifold and pulsar line-of-sight are orthogonal to each other. Hence this phenomenon explains that the projection is very sensitive to the process noise, causing the adverse effect on the results.

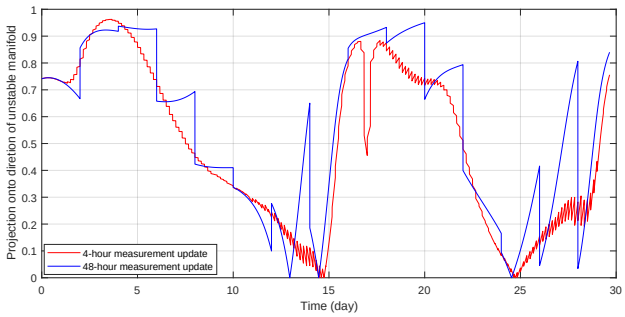

Figure 6: Projection of the estimated error onto the unstable manifold using B1937+21.

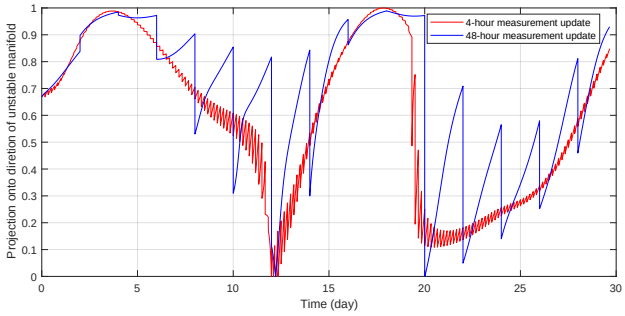

Figure 7: Projection of the maximum orbit uncertainty onto the unstable manifold using B1937+21.

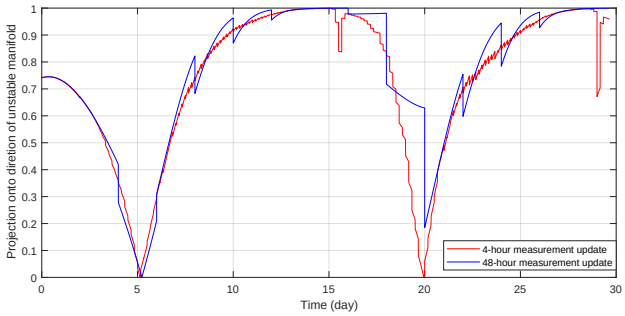

Figure 8: Projection of the estimated error onto the unstable manifold using B1509-58.

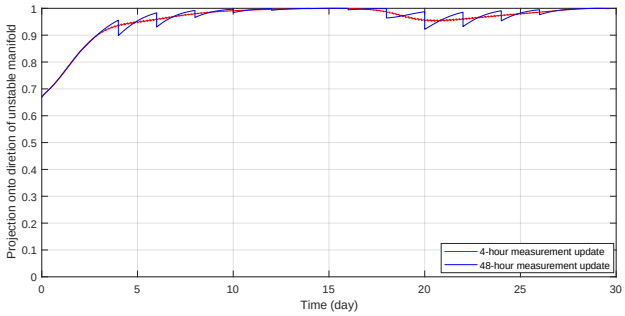

Figure 9: Projection of the maximum orbit uncertainty onto the unstable manifold using B1509-58.

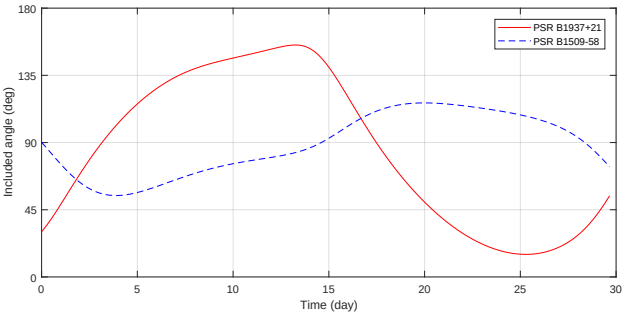

Figure 10: Angle between the direction of the unstable manifold and the pulsar line-of-sight.

5.3. Results for orbit maintenance

This section demonstrates the effectiveness of proposed covariance-based orbit maintenance approach. The duration of the nominal trajectory is 180 days (12 periods in synodic frame). The initial orbit derivation follows zero-mean normal distribution with $\sigma_x = \sigma_y = \sigma_z = 1$ km and $\sigma_{\dot{x}} = \sigma_{\dot{y}} = \sigma_{\dot{z}} = 1$ cm/s. In contrast to the previous simulation, measurement update is performed with observations of B1937+21, B1821-24 and B0531+21 simultaneously. Under above simulation conditions, Monte Carlo simulation is performed for 20 trials.

For the monodromy-based orbit maintenance, the measurement update and maintenance maneuver are performed every 1 hour and 7.5 days, respectively. Figure 11 shows actual trajectory of one of 20 trials. As it is clearly seen, the trajectory is remained near the nominal trajectory for 10 periods (about 150 days) and then diverges away from the nominal trajectory. Figure 12 gives the average maneuver cost of 20 trials. The similar conclusion can be found that the cost increases sharply after 150 days.

For comparison, Fig. 13 shows the results without initial derivation and orbit-determination error. The actual trajectory is almost the same as the nominal one and the total cost is just 9.49×10^{-5} m/s. It is concluded the monodromy-based approach is sensitive to the orbit and measurement uncertainties.

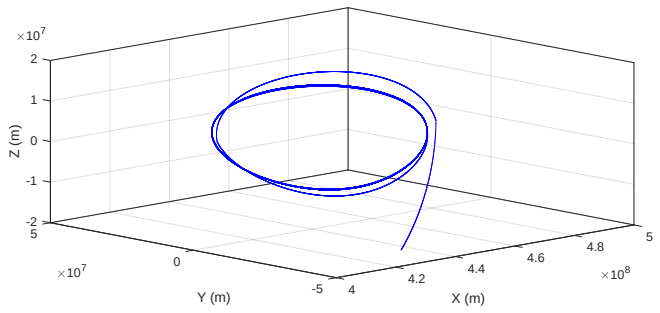

Figure 11: Actual trajectory in synodic frame with the monodromy-based orbit maintenance.

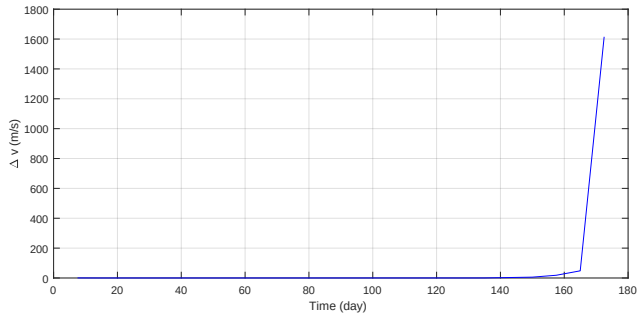

Figure 12: Average cost of each maneuver for 20 trials.

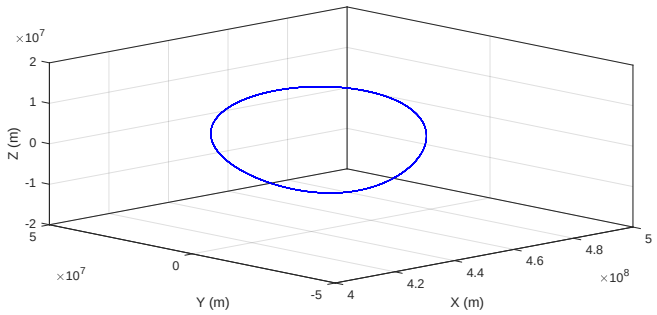

Figure 13: Actual trajectory in synodic frame with the monodromy-based orbit maintenance without initial derivation and orbit-determination error.

Next, the results for the covariance-based approach are shown. The statistic results is summarized in Table 2, where Int_{om} and Int_{mp} denote the interval between the execution of neighbour maneuvers and measurement update, δv_{total} is the total cost of maintenance maneuvers, and Ave and Range are the mean and range of δv_{total} among 20 times simulation. In the cases of 4-hour and 6-hour intervals of maneuvers, the average cost is almost the same. However, according to the range of the maneuver cost, results with 4-hour interval is more stable than that with 6-hour interval. On the other hand, if the maneuver interval is fixed, interval of measurements seems to have no effect on the results. Unexpectedly, the total cost is clearly increased when maneuver interval rises to 12 hours. Results arbitrarily chosen from 20 trials with 12-hour maneuver

Table 2: Statistic results of covariance-based orbit maintenance

Int_{om}	Int_{mp}	δv_{total}	
		Ave	Range
4 hours	2 hours	2.449 m/s	2.014-3.629 m/s
	4 hours	2.534 m/s	2.144-3.433 m/s
6 hours	2 hours	2.481 m/s	1.779-4.198 m/s
	3 hours	2.519 m/s	1.719-4.484 m/s
	6 hours	2.460 m/s	1.564-3.930 m/s
12 hours	2 hours	16.587 m/s	2.085-36.795 m/s
	3 hours	18.554 m/s	3.486-43.538 m/s
	6 hours	12.925 m/s	1.714-51.062 m/s
	12 hours	15.933 m/s	3.625-41.982 m/s

interval and 2-hour measurement maneuver are shown in Figs. 14 and 15.

The actual trajectory is still near the nominal one, however, the cost for each maneuver is increased over time. It is possible that actual trajectory diverges far away from the nominal one in the future. The opposite results, shown in Figs. 16 and 17 with 4-hour maneuver interval and 2-hour, are stable during the whole period. Therefore, the results verifies that the covariance-based approach with smaller maneuver interval has stronger adaptivity to the orbit and measurement uncertainties with smaller cost, while the monodromy-based approach cannot accommodate uncertainties.

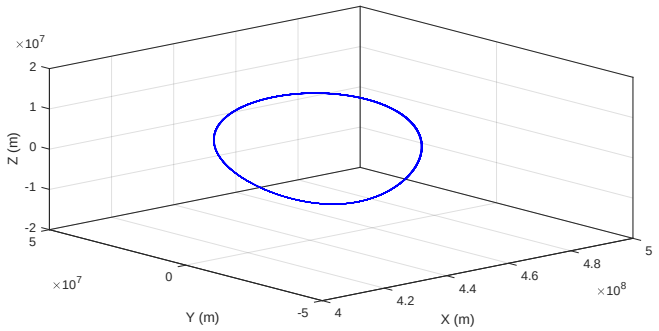

Figure 14: Actual trajectory in synodic frame (Int_{om} = 12 hours and Int_{mp} = 2 hours).

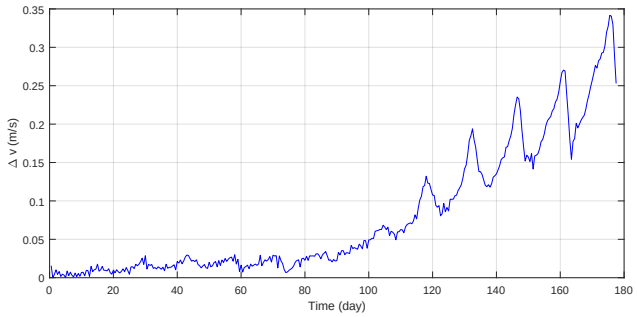

Figure 15: Cost of each maneuver ($\text{Int}_{om} = 12$ hours and $\text{Int}_{mp} = 2$ hours).

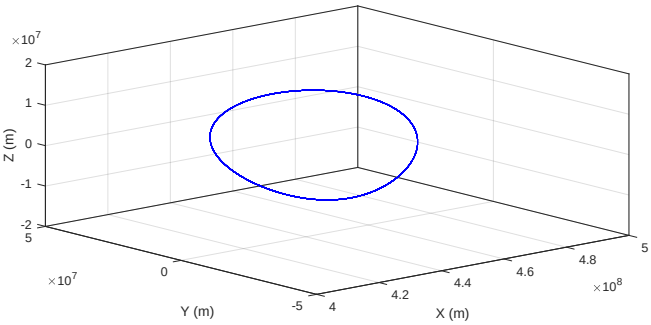

Figure 16: Actual trajectory in synodic frame ($\text{Int}_{om} = 4$ hours and $\text{Int}_{mp} = 2$ hours).

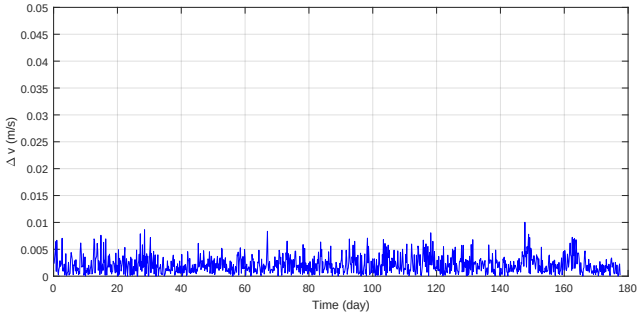

Figure 17: Cost of each maneuver ($\text{Int}_{om} = 4$ hours and $\text{Int}_{mp} = 2$ hours).

6. Conclusions

This paper investigates the integrated orbit determination and orbit maintenance approach for spacecraft in unstable dynamics environments. In contrast to the case in the stable dynamics environment, the distribution of orbit uncertainty in the unstable dynamics environment is dominated by the unstable manifold. When the XNAV measurements are included into orbit determination, measurement from different pulsars show different measurement efficiency, which is closely related to the unstable manifold. Then a new orbital maintenance strategy is proposed using the limiting direction of uncertainty. The maintenance maneuver is designed to force the projection of the derivation from the nominal trajectory onto the unstable direction to be zero so that the derivation converges to zero, instead of being stretched along the unstable direction. By integration with the orbit determination, the covariance matrix is directly obtained by the filter and the computation of monodromy matrix is not required. Simulation results show the spacecraft can be remained in the vicinity of the nominal trajectory with the covariance-based orbit maintenance approach. The future work includes validation of the integrated orbit determination and maintenance approach in more realistic environment, e.g. under the ephemeris model.

References

[1] R. H. Battin, An Introduction to the Mathematics and Methods of Astrodynamics, revised edition Edition, American Institute of Aeronautics and Astronautics, 1999.

[2] O. Montenbruck, E. Gill, Satellite Orbits: Models, Methods, Applications, Springer, 2000.

[3] J. L. Junkins, M. F. Akella, K. T. Alfriend, Non-gaussian error propagation in orbit mechanics, Journal of Astronautical Sciences 44 (4) (1996) 541–563.

[4] D. J. Scheeres, D. Han, Y. Hou, Influence of unstable manifolds on orbit uncertainty, Journal of Guidance, Control, and Dynamics 24 (3) (2001) 573–585.

[5] D. J. Scheeres, Navigation of spacecraft in unstable orbital environments, in: Libration Point Orbits and Applications, World Scientific, 2003, pp. 399–438.

[6] D. J. Scheeres, M. W. Lo, Integrated trajectory and navigation design in unstable orbital environments, Tech. Rep. IPN PR 42-150, InterPlanetary Network Progress Report (April-June 2002).

[7] R. W. Farquhar, D. P. Muhonen, C. R. Newman, H. S. Heubergerg, Trajectories and orbital maneuvers for the first libration-point satellite, Journal of Guidance, Control, and Dynamics 3 (6) (1980) 549–554.

[8] D. W. Dunham, C. E. Roberts, Stationkeeping techniques for libration-point satellites, Journal of the Astronautical Sciences 49 (1) (2001) 127–144.

[9] C. Renault, D. Scheeres, Optimal placement of statistical maneuvers in an unstable orbital environment, in: AIAA/AAS Astrodynamics Specialist Conference and Exhibit, 2002, p. 4725.

[10] K. C. Howell, B. T. Barden, M. W. Lo, Application of dynamical systems theory to trajectory design for a libration point mission, Journal of Astronautical Sciences 45 (2) (1997) 161–178.

[11] S. I. Sheikh, The use of variable celestial x-ray sources for spacecraft navigation, Ph.D. thesis, University of Maryland (2005).

[12] J. Liu, J. C. F. andZ. W. Kang, J. Wu, X. L. Ning, Novel algorithm for x-ray pulsar navigation against doppler effects, IEEE Transactions on Aerospace and Electronic Systems 51 (1) (2015) 228–241.

[13] K. D. Anderson, D. J. Pines, Methods of pulse phase tracking for x-ray pulsar based spacecraft navigation using low flux pulsars, in: SpaceOps 2014 Conference, Pasadena, USA, 2014, pp. 1–23.

[14] P. Graven, J. Collins, S. Sheikh, J. Hanson, P. Ray, K. Wood, Xnav for deep space navigation, in: 31st Annual AAS Guidance and Control Conference, Breckenridge, USA, 2008, pp. 1–16.

[15] Y. J. Qian, C. Y. Li, W. X. Jing, I. Hwang, J. Wei, Sunearthmoon autonomous orbit determination for quasi-periodic orbit about the translunar libration point and its observability analysis, Aerospace Science and Technology 28 (1) (2013) 289–296.

[16] Y. Zhou, P. L. Wu, X. X. Li, Adaptive navigation algorithm under abnormal measurements in libration-point mission, IEEE Transactions on Aerospace and Electronic Systems 54 (1) (2018) 246–256.

[17] G. Gomez, K. C. Howell, J. Masdemont, C. Simo, Station-keeping strategies for translunar libration point orbits, Advances in Astronautical Sciences 99 (2) (1998) 949–967.

[18] R. Farquhar, The control and use of libration point satellites, Tech. Rep. TR R346, NASA Technical Report (1970).

[19] R. W. Farquhar, D. P. Muhonen, C. R. Newman, H. S. Heuberger, Trajectories and orbital maneuvers for the first libration-point satellite, Journal of Guidance, Control, and Dynamics 3 (6) (1980) 549–554.

[20] K. C. Howell, H. J. Pernicka, Station-keeping method for libration point trajectories, Journal of Guidance, Control, and Dynamics 16 (1) (1993) 151–159.

[21] T. Pavlak, K. C. Howell, Strategy for optimal, long-term stationkeeping of libration point orbits in the earth-moon system, in: AIAA/AAS Astrodynamics Specialist Conference, Minnesota, USA, 2012, pp. 1–16.

[22] C. Simo, G. Gomez, J. Llibre, R. Martinez, J. Rodriguez, On the optimal station keeping control of halo orbits, Acta Astronautica 15 (6) (1987) 391–397.

[23] Y. Sugimoto, Y. Kawakatsu, T. Saiki, Orbit maintenance maneuver for lagrange point missions using dst in sun-earth er3bp, Advances in the astronautical sciences 153 (1) (2015) 91–100.

[24] C. Marchal, The three-body problem, Elsevier, 2012.

[25] G. J. Bierman, C. L. Thornton, Numerical comparison of kalman filter algorithms: Orbit determination case study, Automatica 13 (1) (1977) 23–35.

[26] H.Schaub, J. L. Junkins, Analytical Mechanics of Space Systems, American Institute of Aeronautics and Astronautics, 2014.

[27] Y. Sunahara, K. Yamashita, An approximate method of state estimation for non-linear dynamical systems with state-dependent noise, International Journal of Control 11 (6) (1970) 957–972.

[28] S. I. Sheikh, D. J. Pines, P. S. Ray, K. S. Wood, M. N. Lovellette, M. T. Wolff, Spacecraft navigation using x-ray pulsars, Journal of Guidance, Control, and Dynamics 29 (1) (2006) 49–63.

[29] S. I. Sheikh, D. J. Pines, Recursive estimation of spacecraft position and velocity using xray pulsar time of arrival measurements, NAVIGATION: Journal of The Institute of Navigation 53 (3) (2006) 149–166.

[30] J. E. Prussing, B. A. Conway, Orbital Mechanics, second edition Edition, Oxford Unicersity Press, 2013.

[31] Y. Sugimoto, Trajectory design for lagragne point missions using dst in restricted three-body problem, Ph.D. thesis, The Graduate University for Advanced Studies (2015).

[32] D. L. Richardson, Analytic construction of periodic orbits about the collinear points, Celestial Mechanics and Dynamical Astronomy 22 (3) (1980) 241–253.

[33] K. C. Howell, Three-dimensional, periodic, halo orbits, Celestial Mechanics and Dynamical Astronomy 32 (1) (1984) 53–71.

[34] Y. Zhou, M. Bando, S. Hokamoto, P. L. Wu, Influence of unstable dynamics on orbit determination with x-ray pulsar navigation, in: DyCoSS 2018, Changsha, China, 2018, pp. 1–17.